Journal of the American College of Cardiology
© 2006 by the American College of Cardiology Foundation
Published by Elsevier Inc.

Vol. 48, No. 10, 2006
ISSN 0735-1097/06/$32.00
doi:10.1016/j.jacc.2006.06.071

Assessment of Left Ventricular Function by Cardiac Ultrasound

James D. Thomas, MD, Zoran B. Popović, MD, PHD
Cleveland, Ohio

Our understanding of the physical underpinnings of the assessment of cardiac function is becoming increasingly sophisticated. Recent developments in cardiac ultrasound permit exploitation of many of these newer physical concepts with current echocardiographic machines. This review will first focus on the current approach to the assessment of cardiovascular hemodynamics by cardiac ultrasound. The next focus will be the assessment of global cardiac mechanics in systole and diastole. Finally, relationships between the cardiac structure and regional myocardial function, and the way regional function can be quantified by ultrasound, will be presented. This review also discusses the clinical impact of echocardiography and its future directions and developments. (J Am Coll Cardiol 2006;48: 2012–25) © 2006 by the American College of Cardiology Foundation

Our understanding of the physical underpinnings of the assessment of cardiac function is becoming increasingly sophisticated. Recent developments in cardiac ultrasound permit exploitation of many of newer physical concepts with current echocardiographic equipment. We will review the current approach to the assessment of cardiac function and hemodynamics by ultrasound, its clinical impact, and discuss some of the future directions. Due to space limitations, we will not be able to discuss the relative role of echocardiography versus other imaging modalities, except to note that, utilized to its fullest potential, it is the most cost-effective way of assessing overall ventricular and valvular function. Also, the incremental contribution of stress echocardiography will not be specifically discussed; however, the principles of the techniques discussed in this review are valid during and after exercise and pharmacologic stress, and can be applied in this arena. The reader is referred to a recent excellent review on the subject (1).

CARDIAC HEMODYNAMICS

We turn first to indexes of blood flow in the heart. Blood flow is governed by conservation of mass, momentum, and energy. Together these conservation laws form the basis for the echocardiographic assessment of cardiac hemodynamics. To understand the practical applications of quantitative echocardiographic methods, it is helpful to review the basis for these laws and how they relate to the empiric parameters of interest to cardiologists.

From the Department of Cardiovascular Medicine, The Cleveland Clinic Foundation, Cleveland, Ohio. Supported by grants from the National Institutes of Health (grant AG17479-02), the National Space Biomedical Research Institute through NASA NCC 9-58 (Houston, Texas), the Department of Defense (Ft. Dietrick, Maryland, USAMRMC grant No. 02360007), the National Institutes of Health, National Center for Research Resources, General Clinical Research Center (grant MO1 RR-018390), and by a National American Heart Association grant (0235172 N).

Manuscript received March 2, 2006; revised manuscript received June 2, 2006, accepted June 19, 2006.

Conservation of mass. Conservation of mass implies that blood can neither be created nor destroyed. Because blood is incompressible, it means that flow into any region of the heart must be matched by flow out of that region. A practical application is the continuity equation for measuring cardiac flow, stroke volume (SV), and cardiac output. For example, if we assume that velocity across the left ventricular outflow tract (LVOT) is constant, then instantaneous cardiac output will be given by flow velocity (from pulsed wave [PW] Doppler) multiplied by LVOT area (2,3). Integrating the velocity throughout systole before multiplying it yields SV; multiplying SV by heart rate yields cardiac output. In practice, error may be introduced by the fact that the velocity profile across the LVOT is not flat (4) but tends to be skewed toward the septum, but even the simple calculation outlined here is reasonably accurate and should be applied routinely in clinical echocardiography to provide cardiac output. Semiautomated methods have been validated to integrate the color Doppler velocities across the LVOT to yield SV with fewer assumptions, but unfortunately these are not widely available (5).

In the absence of shunts or regurgitation, the same SV should be obtained by measuring flow through any other structure of the heart as long as the velocity and area are measured at the same point. The tricuspid (6), pulmonary, and mitral annuli (7) are candidates for these measurements, although the LVOT is most reliable. If regurgitation or shunt flow is present, then any discrepancy in flow in different regions of the heart reflects the shunt (8,9) or regurgitant volume (RV) (10). All that is necessary is for one of the flows to reflect the net forward output of the heart. For example, if an atrial septal defect is present, LVOT SV might be 80 ml, whereas pulmonic SV might be 120 ml, in which case shunt volume would be 40 ml with a shunt fraction of 1.5:1. In the case of mitral regurgitation, mitral annular SV of 100 ml and LVOT SV of 60 ml indicate mitral RV of 40 ml.

Abbreviations and Acronyms

DTI = Doppler tissue imaging
EF = ejection fraction
LV = left ventricle/ventricular
LVOT = left ventricular outflow tract
PW = pulsed wave
ROA = regurgitant orifice area
RV = regurgitant volume
STI = speckle tracking imaging
SV = stroke volume
2(3)D = 2(3)-dimensional

Measurement of left and right heart SV is currently standard clinical method to quantitate shunts. Measurement of RV is less used because it is more prone to measurement errors, particularly because 2 large SVs are subtracted from each other to yield a much smaller RV; this prompted development of more direct approaches, such as the proximal convergence method.

The proximal convergence method is also based on conservation of mass. It states that all flow passing through a regurgitant valve approaches it as a series of concentric shells of decreasing surface area and increasing velocity (11). Quantifying flow through any such shell (most conveniently the contour identified by velocity aliasing in the color Doppler display) yields the instantaneous flow through the valve. Assuming this contour to be hemispheric in shape, then flow Q through a contour of velocity v_a at radius r from the regurgitant orifice is $2\pi r^2 v_a$. If the velocity through that orifice at that instant is v_0, then the important parameter regurgitant orifice area (ROA) is given by Q/v_0 (12). For mitral regurgitation, this can be simplified by assuming a regurgitant velocity of 5 m/s (reflecting a ventriculoatrial pressure difference of 100 mm Hg). If aliasing velocity is set to 40 cm/s, then ROA will be given simply by $r^2/2$ (13) (Fig. 1).

In practice, the shape of proximal convergence shell may deviate from a hemispheric one, especially during states of low flow (14), distortion by adjacent walls (15), and irregular orifices. Also, when regurgitation is mild, an aliasing contour often may not be measurable, but this absence alone is helpful in reassuring one of the trivial magnitudes of the regurgitation.

Conservation of energy. Energy exists in many forms inside the heart: pressure, kinetic energy of blood flow, the sound of murmurs, and so on. Conservation of energy states that the total energy within a closed system (like the heart) must be a constant. In practical terms, we can use the balance between kinetic (i.e., velocity) and potential (i.e., pressure) energy to estimate the pressure drop across stenotic valves and other restrictive orifices. The kinetic energy within a sample volume is given by $1/2\rho v^2$. As blood moves into a stenotic valve, the velocity must increase (by the continuity equation), and as the kinetic energy increases, the local pressure must fall. In its full form, this balance between potential and kinetic energy is the complete Bernoulli equation with multiple complex terms, but for flow through a restrictive orifice with velocity measured in m/s, the pressure drop in mm Hg will be given by the simplified formula, $\Delta p = 4v^2$ (16) (Fig. 2). There are many caveats to the simplified Bernoulli equation: 1) it does not apply to long tunnel-like stenoses where viscosity contributes to the pressure drop (17); 2) it does not apply to non-restrictive orifices because most of the pressure drop is used in accelerating the bulk of the blood through the valve and is quantified by the inertial term of the complete Bernoulli equation (18,19); and 3) it may overestimate the net

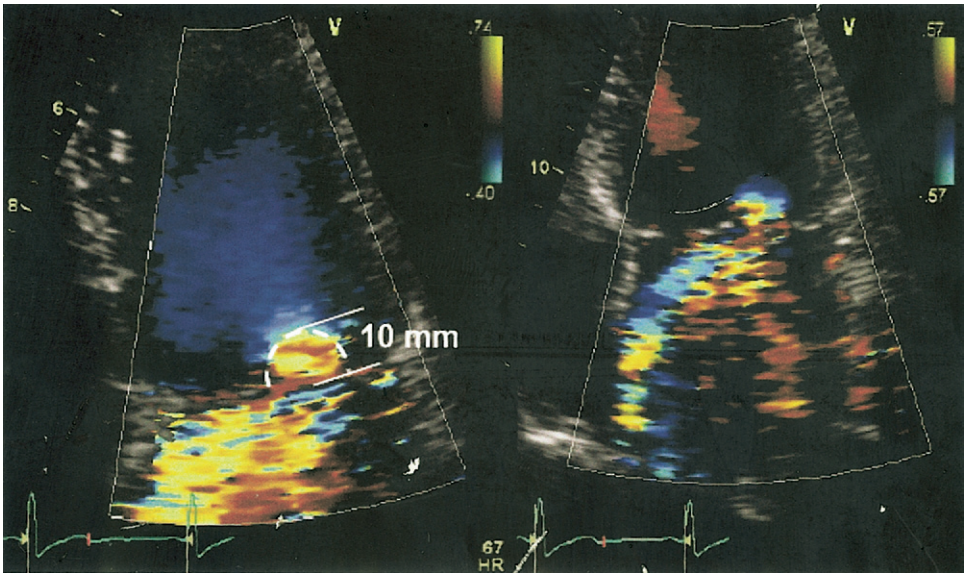

Figure 1. Principle of the conservation of mass. Instantaneous flow through the shell outlined by the proximal isovelocity surface is identical to the regurgitation flow rate occurring through this insufficient mitral valve. To the **right**, the same valve shows a highly asymmetric regurgitation jet whose area underestimates the true amount of regurgitation.

JACC Vol. 48, No. 10, 2006
November 21, 2006:2012–25

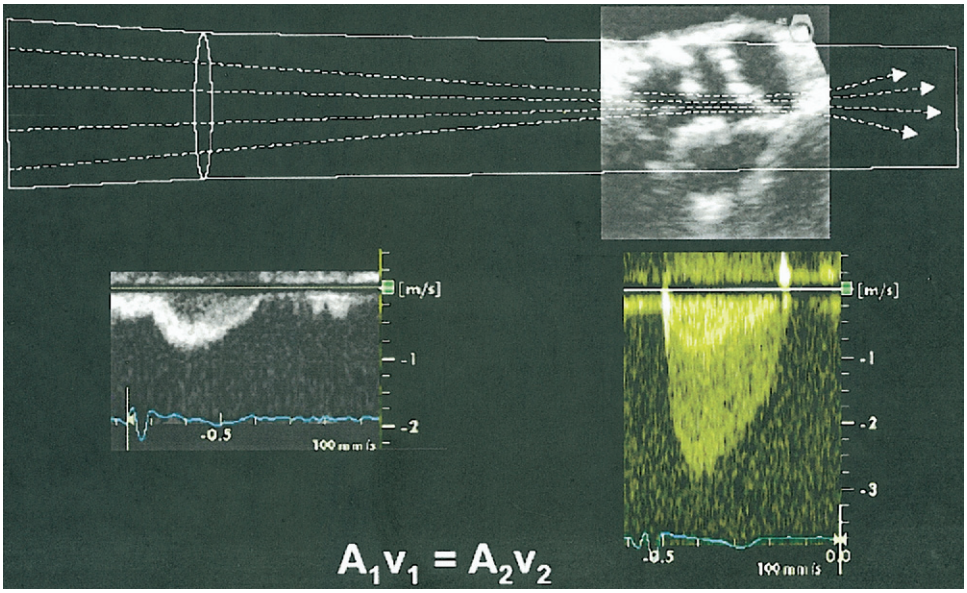

Figure 2. Principle of the conservation of energy. Decrease of cross-sectional area (as seen in aortic stenosis) leads to increase in velocity. Velocity increase leads to a pressure decrease distal to the stenosis.

pressure drop through bileaflet prosthetic valves, where the pressure energy decrease as the kinetic energy rises is not irretrievably lost, but rather partially recovered as the flow smoothly decelerates out of the prosthesis (20). Despite these limitations, it is remarkable how well the simplified Bernoulli equation works, having been validated for stenotic native valves, prosthetic valves, valvular regurgitation, and restrictive intracardiac shunts and likely is the single development that most propelled Doppler echocardiography into the premiere cardiac imaging modality it is today. Currently, it represents the gold standard for the measurement of valve stenoses (21).

Conservation of momentum. If we consider flow with velocity v through an orifice with area A, conservation of mass in fluid terms really means conservation of mass flux, or simply flow, Q = Av. The kinetic energy flux (used in the Bernoulli equation) then is given by $1/2\rho(Av)v^2$. There is a third conserved quantity, momentum, which flux is given by $\rho(Av)v$. Though less familiar to cardiologists, momentum is important, because it is the physical entity that best predicts the size of a regurgitant jet on color Doppler imaging (22). From its definition, it is clear that even if jet flow remains constant, increasing the velocity of the jet (as by increasing the driving pressure) will increase apparent jet size, explaining the importance of knowing blood pressure when interpreting color Doppler images. Though it is theoretically possible to quantify the momentum across a jet cross section to characterize its severity (23), this is limited in practice by the presence of high velocity turbulence within the jet.

CARDIAC MECHANICS

The echocardiographic assessment of cardiac mechanics can be divided into methods that quantify global function and those that assess regional contractility.

Echocardiographic assessment of global LV chamber function: ejection fraction (EF), contractility, relaxation, filling, and end-diastolic pressure. In contrast to the fluid dynamics of blood motion around the cardiovascular system, the structural mechanics principles that apply to the assessment of systolic and diastolic chamber function are more complex. Thus, one of the biggest challenges is simply deciding how best to quantify cardiac function. From an operational point of view, adequate cardiac function is the ability of the heart to fill at a low enough pressure not to cause pulmonary congestion, then deliver a sufficient quantity of blood to the vasculature at a high enough pressure to perfuse the tissue, and to augment this performance during exercise. Unfortunately, there is no measurable quantity that corresponds to this integrated functional assessment, so we must use surrogates that approximate one or another aspect of cardiac function.

LV volumes and EF. The most common functional surrogate is LVEF, the percentage of chamber volume ejected in systole, which is well measured by echocardiography. The first step in calculating LVEF is correct visualization of endocardial borders. Although in most cases this can be done by standard approach, it is sometimes necessary to use ultrasound contrast for LV opacification; this is especially true in the morbidly obese, in the presence of apical masses, and during stress echocardiography (24). To obtain LV volumes and EF, one can use formulae that have been validated for M-mode measurements and single and biplane 2-dimensional (2D) assessments, but these are based on geometric assumptions and so work best in symmetric ventricles (25–27). Methods have been developed for more automated estimation of EF from 2D echocardiograms. Acoustic quantification analyzes the intensity of the returning ultrasound signal to separate the ventricle into tissue and

blood and track LV area in real-time (28). By assuming rotational symmetry, end-systolic and end-diastolic volumes can be estimated on a beat-by-beat basis, along with EF. Color kinesis extends this principle by tracking the LV endocardial contour frame-by-frame, allowing the time course of filling and ejection to be displayed (29). However, although these methods are very accurate in tracking the relative changes of LV volumes throughout cardiac cycle, the absolute values still need to be calibrated (30). For maximal accuracy, particularly with ventricular aneurysms or other asymmetric abnormalities, 3-dimensional (3D) echocardiography should be used, which has an accuracy rivaling magnetic resonance imaging (31,32).

Currently, there are 3 broad approaches to 3D echocardiography. The first is 3D reconstruction from a set of 2D planes obtained by either rotating or tilting the transducer, a method that is time consuming and requires stable heart rate, but can be done with conventional 2D transducers. The second approach is real-time 3D echocardiography, which uses an array of crystals to direct ultrasound anywhere within a pyramid of space. Despite parallel processing (typically ~16:1), this often requires combining data from 3 to 5 cardiac cycles to obtain a full 90° × 90° 3D pyramid. Finally, much of the quantitative accuracy of full 3D echocardiography can be obtained from transducers capable of simultaneously acquiring up to 3 rotationally arranged planes. An important technical issue involves the number of slices from which the ventricular volume (or mass) is measured, ranging from 2 (33) to 12 (34), with accuracy falling when the number of planes is <4 (35). Arguing against too many slices is the time and effort required for analysis. Fortunately, software is emerging that can (semi) automatically detect endocardial borders during a cardiac cycle (34,36).

There is no current consensus on when to perform 3D echocardiography in clinical practice, although the American Society of Echocardiography is soon to release a guidelines document. This is partly due to the rapid evolution of this novel technology and the absence of a comprehensive industry-wide format in which to store the data, which would allow more options in post-processing and visualization. The Digital Imaging and Communications in Medicine committee is pursuing such a standard, but progress has been slow. However, because data acquisition is brief, adding little to the cost or inconvenience of an examination, a strong case can be made for using 3D echocardiography to document serial changes in LV (or any other chamber) volume, particularly for clinical scenarios such as asymptomatic mitral and aortic regurgitation, and assessment of cardiac resynchronization therapy.

Contractility. Although EF is universally used, it is limited by its sensitivity to preload and afterload, exemplified by the false reassurance of a high EF in severe mitral regurgitation and the low, but reversible, EF with severe aortic stenosis. Because of this, much effort is given to developing less load-dependent methods to measure true contractility, the most accurate of which requires continuous acquisition of ventricular pressure and volume data during sudden preload change. From these data, several indexes can be calculated, with end-systolic elastance (37) and preload recruitable stroke work being the most popular. Many studies have sought non-invasive echocardiographic estimates of these parameters that can be obtained without preload intervention.

Kass et al. (38) have suggested that LV power (a product of peak systolic flow and pressure), indexed to the square of end-diastolic volume, accurately estimates end-systolic elastance, although later work suggests that this type of correction is inadequate (39,40). A more direct approach by the same group estimated end-systolic elastance from a single beat using a complex combination of non-invasive measurements of blood pressures, diastolic and systolic LV volumes, pre-ejection and ejection times, and EF (41,42). A similar single-beat estimate was developed for preload recruitable stroke work.

Several other groups used empirical approaches to estimate end-systolic elastance echocardiographically. For example, we have shown that systolic velocity acceleration in the LVOT (43) and systolic strain rate (44) correlate with end-systolic elastance. Similarly, it has been shown that the early systolic intraventricular pressure drop along the LVOT (45) correlates with end-systolic elastance (for calculation, see the following text). Another proposed contractility parameter is myocardial performance index, obtained by dividing the sum of isovolumic contraction and relaxation times with ejection time. However, although studies have shown its clinical value (46), its usefulness as contractility parameter is debatable (47). Similarly, a claim that isovolumic acceleration by Doppler tissue imaging (DTI) is a good marker of end-systolic elastance (48) has recently been heavily contested (49).

Assessment of regional myocardial contraction. Regional function is commonly assessed by dividing the LV into 17 segments (recently agreed to by the echocardiographic, nuclear, and magnetic resonance communities) and assigning a qualitative grade to each ranging from 1 (normal) to 5 (aneurysmal) (50). This method had changed little from the initial descriptions of wall motion abnormalities by echocardiography (51) and is observer-dependent. However, novel insights into myocardial structure and new echocardiographic modalities may dramatically change the way we assess regional function.

Myocardial structure and myocyte shortening. Myocytes lie in planes parallel to the long axis of the heart. Within these planes, myocyte orientation varies. It is circumferential at the mid-wall, but rotates clockwise (as viewed from the outside) to form a −60° left-handed helix in the epicardium and counterclockwise to a +60° right-handed helix in endocardium (Fig. 3A) (52). Myocytes are organized into sheets 4 cells thick (53) that are stacked shingle-like (52) (Fig. 3A), transducing a 14% decrease in myocyte length to 40% thickening of the LV wall (54) by increasing sheet angles during systole (Fig. 3B) (52,54–56). Also, myocytes

JACC Vol. 48, No. 10, 2006
November 21, 2006:2012–25

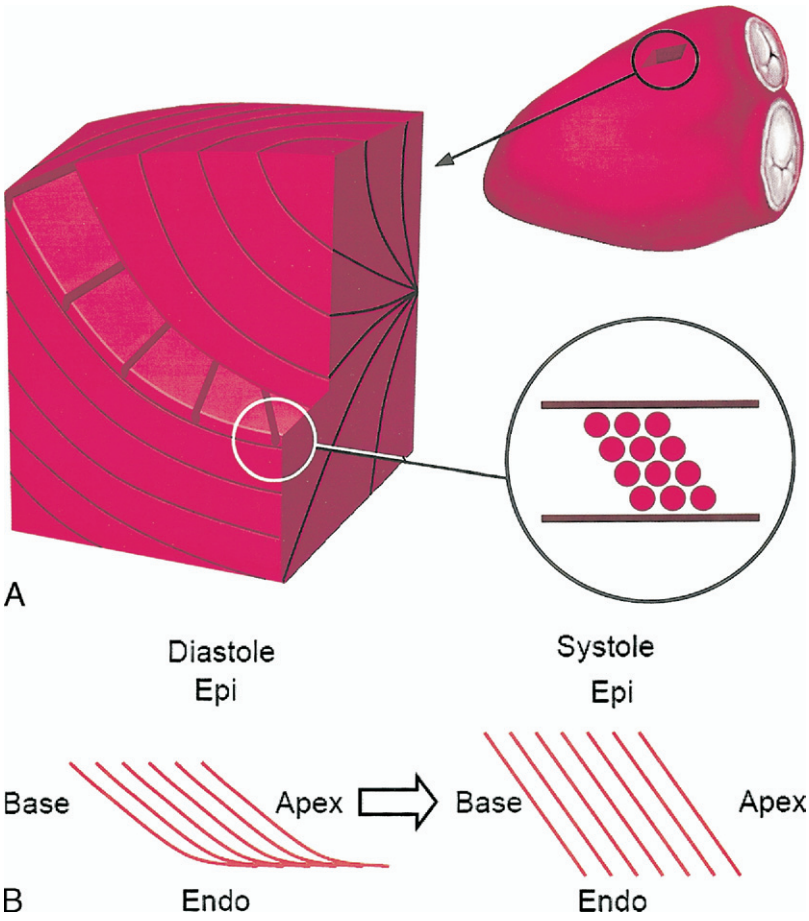

Figure 3. **(A)** Myocardial fiber and sheet orientation within a block of muscle excised from the anterior wall of the left ventricle. Myocytes lie in planes parallel to the long axis of the heart. Within these planes, myocyte orientation is circumferential at the mid-wall, but rotates clockwise (when viewed from the outside) to form a −60 degree left-handed helix in the epicardium (Epi) and counterclockwise to a +60° right-handed helix in endocardium (Endo). Myocytes are organized into sheets 4 cells thick that are stacked like shingles. **(B)** Myocardial sheet movement during cardiac cycle. During systole, due to rearrangement of myocytes, sheets are becoming more perpendicular toward the endocardium, thus helping to transform a 14% decrease in myocyte length to 40% thickening of the left ventricular wall.

passively shorten due to the action of adjacent areas, and because of the conservation of mass, the subendocardium consistently shortens more than in the subepicardium (Fig. 4) (57). With these issues in mind, it is obvious that new imaging modalities should discriminate between various segments and layers of the heart to fully appraise contractility.

DTI. By eliminating the wall filter and using low-gain amplification, it is possible to display myocardial tissue velocity either as a PW Doppler signal at a specific place in the myocardium, a color map, or an arbitrarily oriented M-mode. Imaged from the apex, it is possible to visualize long-axis motion towards the apex in systole, reversing itself in diastole, with complex biphasic movements during isovolumic periods. Newer machines can simultaneously capture multiple color DTI planes arranged around a common axis. Analysis of such simultaneously acquired DTI data over several LV regions has been used to assess LV synchrony (58–60) and as an additional tool during stress echocardiography (61).

Doppler tissue imaging assessment of contractility has a number of limitations: 1) like all Doppler methods, it can only measure the component of motion parallel to the ultrasound beam; 2) velocity may reflect gross translation (as in right ventricular volume overload) (62), rather than actual local contraction; and 3) even akinetic segments show motion due to tethering of adjacent normally contracting segments.

DTI-derived strain measurements. To overcome the latter 2 problems, DTI-derived strain and strain rate have been recently proposed as new parameters of regional LV function. Strain is a mathematically complex construct (a 3D tensor, represented by a 3 × 3 matrix), reflecting local tissue deformation. Deformation can occur by linear compression or expansion along the x-, y-, or z-axes (termed the linear components and represented by the diagonal elements of the tensor, with negative numbers reflecting compression); deformation can also occur when 1 plane slides relative to an adjacent plane, termed shear and represented in the off-diagonal elements of the tensor. For incompressible tissue-like myocardium, the elements above the diagonal are opposite to those below, so there are only 6 independent elements to the myocardial strain tensor (63). There are a

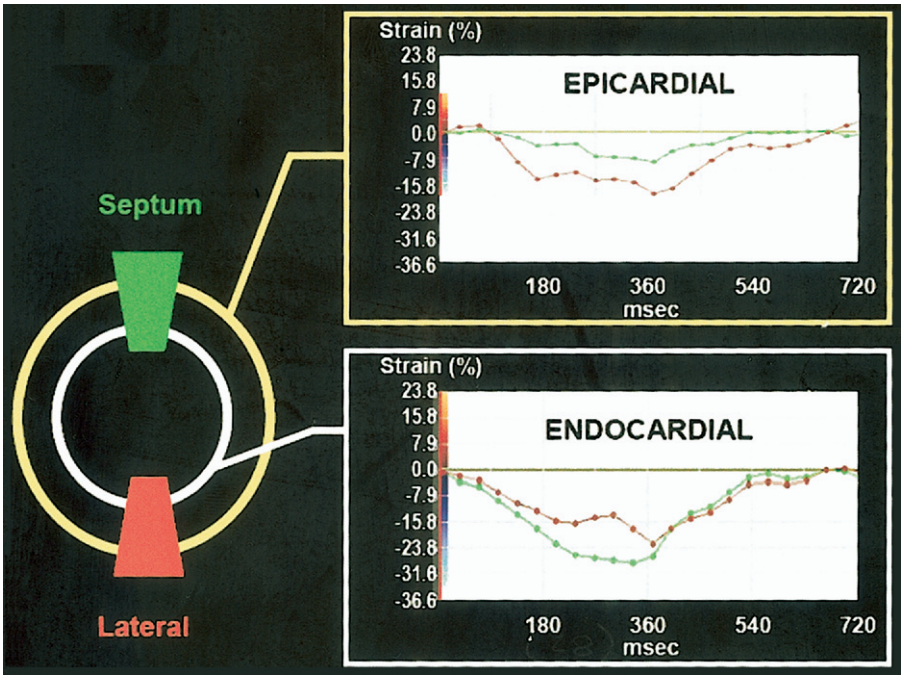

Figure 4. A dramatic difference between endocardial and epicardial shortening (quantitated by measurement of circumferential strains) of the septum and lateral wall in a normal left ventricle detected by speckle tracking imaging.

myriad of different mathematical representations for strain, but cardiology most commonly uses Lagrangian strain (ϵ), a change of dimension divided by the initial dimension, $\Delta L/L_0$, (Fig. 5A) where L_0 is the end-diastolic dimension of a myocardial segment, so ϵ is negative for long-axis strain (myocardium shortens) and positive for radial strain (wall thickening). In actuality, the initial entity calculated from DTI is the strain *rate*, given by the spatial derivative of velocity along a scanline dv/ds, reflecting instantaneous contraction and relaxation of the tissue. Integrating strain rate during systole and performing some further mathematical conversions yields systolic Lagrangian strain. Although strain has been used previously in cardiology for the purpose of diastolic function assessment (64), these older studies bear little connection to this newer resurgence of interest in strain, because they referenced strain to the theoretical unloaded dimensions of the ventricle.

Doppler tissue imaging–obtained strain and strain rate have the time resolution capability far superior to any other non-invasive method (Fig. 5B). Doppler tissue imaging–derived strain accurately measures longitudinal deformation of the heart (65) and is sensitive to early stages of ischemia (66). Strain rate imaging is also useful in the assessment of myocardial viability after infarction (67). Normal age-stratified values for DTI, myocardial displacement (the integral of DTI velocity, reflecting total movement of the myocardium during systole), strain, and strain rate have been published (68). Intuitively, strain rate should be more sensitive to pathology than strain (because prolonged contraction may yield normal strain despite low strain rate), but in practice, strain rate data are noisier, whereas the integration process makes strain data more reproducible. Finally, strain and systolic strain rate show some preload dependency due to their sensitivity on initial diastolic dimension through the Starling mechanism.

Speckle tracking imaging (STI). Doppler tissue imaging–derived strain and strain rate have several limitations. As DTI strain measures only the deformation occurring in the direction of the ultrasound scanline, it yields only a single component of the strain tensor and is very sensitive to transducer orientation, even more so than the usual Doppler angular dependency. In fact, assessing longitudinal contraction at only 45° off of the correct orientation yields zero strain (69). To avoid this angle dependence of all Doppler techniques, STI has recently been introduced. Speckle tracking imaging identifies characteristic speckles within the myocardium and tracks them frame-by-frame to yield tissue deformation in 2 dimensions (Fig. 5C). Speckle tracking imaging is independent of transducer orientation and allows accurate display of tissue velocity, strain rate, strain, and a host of other derived parameters in 2 orthogonal dimensions. Recent studies have shown good accuracy (70) and usefulness in the clinical setting (71).

Strain and strain rate assessment by either DTI or STI are still relatively new and evolving technologies. Clinical conditions emerging as especially suitable to these modalities are regional function assessment at rest (72), during stress echocardiography (73), during acute ischemia (74), and for detecting viability (75).

Assessment of diastolic function. With respect to cardiovascular performance at rest and exercise, of equal importance to systolic function is diastolic function, the ability of the ventricle to fill at low left atrial pressure. Echocardiographic assessment of diastolic function begins with record-

JACC Vol. 48, No. 10, 2006
November 21, 2006:2012–25

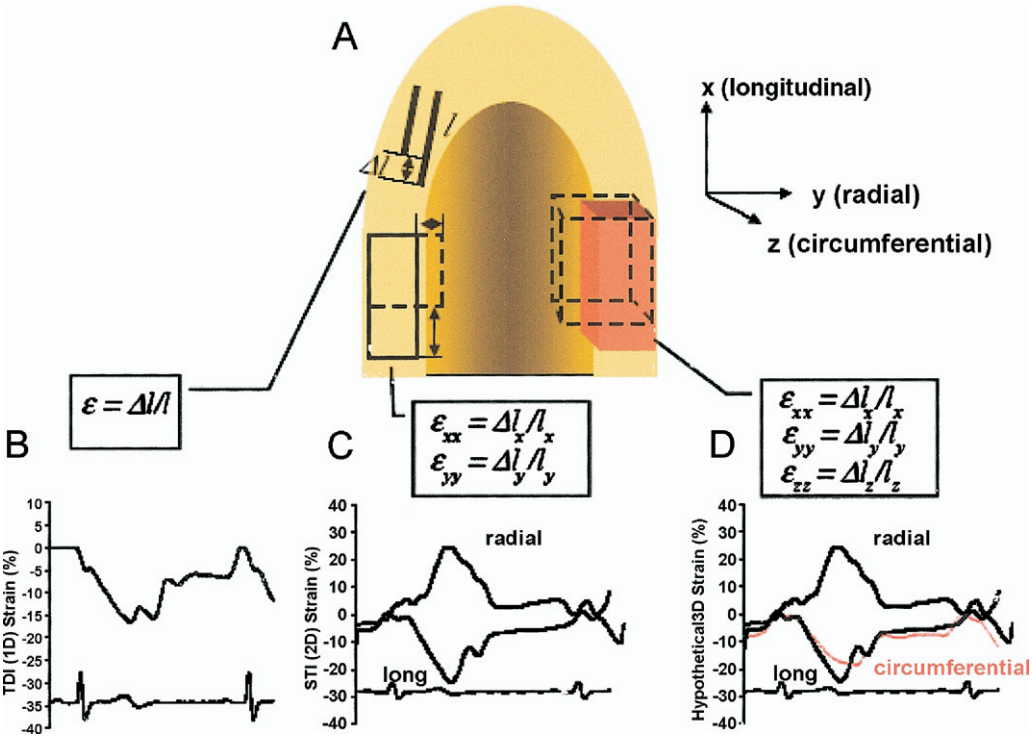

Figure 5. **(A)** One-, 2-, and 3-dimensional representation of linear myocardial strains. **(B)** One-dimensional strain obtained by tissue Doppler imaging (TDI). **(C)** Two-dimensional strain obtained by speckle tracking imaging (STI). **(D)** A hypothetical strain that could be obtained by STI analysis of 3-dimensional data set.

ing the transmitral filling pattern via pulsed Doppler at the mitral leaflet tips. Normally, the early filling wave (E) is larger than the A-wave of atrial contraction, but with LV hypertrophy and other pathologies commonly seen with aging, the E/A ratio falls below 1, termed delayed relaxation. Theoretical (76), in vitro (77), animal (78), and clinical studies have shown that the acceleration of the E wave (and for the most part its maximal velocity) is proportional to left atrial pressure divided by τ, the exponential time constant of isovolumic LV pressure fall. With progressive diastolic dysfunction, compensatory mechanisms to preserve SV yield higher left atrial pressure, reversing the delayed relaxation pattern to the pseudonormal one, with E/A >1 (79). At end-stage, the ventricle fills only at a very high pressure and on a steep (and stiff) portion of the diastolic pressure-volume curve, yielding the restrictive

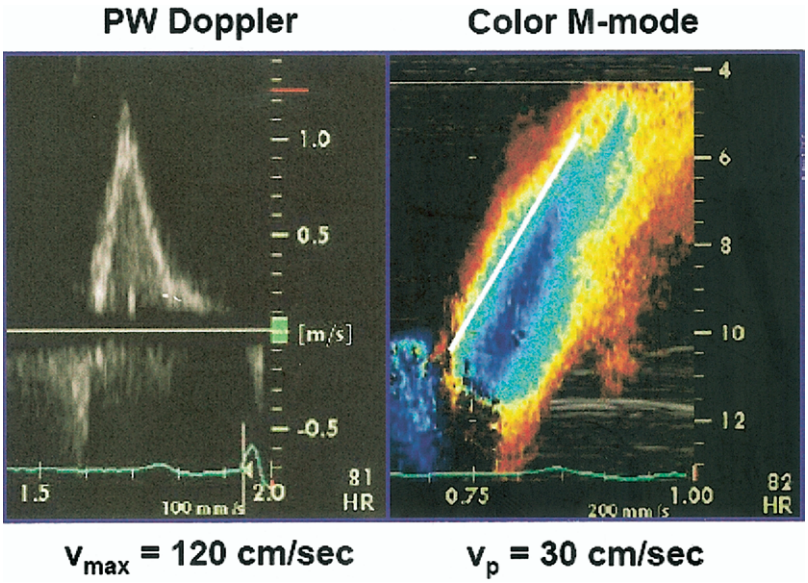

Figure 6. An example of the mismatch between high transmitral E-wave velocity (v_{max}; **left**) and flow propagation velocity (v_p) occurring in a patient with a heart failure and elevated preload. PW = pulsed wave.

Table 1. Classification of Diastolic Dysfunction: Standard and New Criteria

	Delayed Relaxation	Pseudonormal Filling	Restrictive Filling
Standard criteria			
Mitral inflow			
E/A	<1	1–2	>2
DT (ms)	>200	150–200	<150
IVRT (ms)	>100	60–100	<60
Pulmonary vein flow			
S/D	>1	<1	<1
AR (cms)	<35	>35*	>25*
"New" criteria			
Vp (cm)	<45	<45	<45
Em (cm/s)	<8	<8	<8
Emerging markers			
E/Asr	(Applicable to regional function)		
IVPD (mm Hg)	<1?	<1?	<1?
Vuntw (rad/s)	<−1?	<−1?	<−1?

*Unless atrial mechanical failure is present.

AR = pulmonary venous atrial contraction reversal velocity; DT = early left ventricular filling deceleration time; E/A = early-to-atrial ventricular filling ratio; E/Asr = early-to-atrial diastolic strain rate ratio; Em = mitral annulus peak early diastolic velocity; IVPG; intaventricular pressure difference; IVRT = isovolumic relaxation time; S/D = systolic-to-diastolic pulmonary flow ratio; Vp = color M-mode flow propagation velocity; Vuntw = peak untwisting velocity.

filling pattern, with E > A, and deceleration time <150 ms, a pattern with an exceedingly poor prognosis (80,81).

Pulmonary venous flow is a helpful adjunct in diastolic function assessment. A recent review summarizes the assessment of pulmonary venous flow (82), the most useful aspect being the size and morphology of the atrial reversal wave that occurs with atrial contraction. Deep and broad reversal waves indicate high ventricular stiffness (83), and the difference between the duration of transmitral and pulmonary venous A waves is predictive of LV end-diastolic pressure (84). Worsening systolic (and diastolic) function is associated with a diminished S wave, but this is also seen with mitral regurgitation and atrial fibrillation.

Transmitral and pulmonary venous flow indexes are sensitive to left atrial pressure (as with the normal and pseudonormal filling patterns), and investigators have sought indexes less sensitive to load. For example, in heart failure, *early diastolic myocardial velocity* by DTI falls with delayed relaxation, but does not rise with compensatory preload adjustment and so can distinguish normal from pseudonormal transmitral flow (85) and constrictive pericarditis from restrictive cardiomyopathy (86).

Color M-mode flow propagation is obtained by directing an M-line from the LV apex through the mitral valve into the left atrium and recording a spatiotemporal map of flow propagating across the mitral valve in diastole, shown to be related to LV relaxation (87) and to be slowed in ischemia and heart failure (88,89). A number of methods have been proposed for estimating the propagation velocity, but we favor simply shifting the color baseline so that aliasing occurs at about 30% to 40% of the maximal transmitral velocity and measuring the slope of the red-blue transition. Values below 45 cm/s tend to be predictive of diastolic dysfunction. Flow propagation velocity is not prone to pseudonormalization with rising filling pressure (90) (Fig. 6). The major pitfalls in assessing color M-mode flow propagation velocity are low reproducibility due, in part, to misalignment of color M-mode cursor and mitral inflow, and misinterpreting very rapid low velocity motion that occurs during isovolumic relaxation as the true propagation velocity. Low reproducibility is more of a problem at high flow propagation velocity, as the base-apex propagation time is short, with high relative error. Automated methods may make flow propagation measurements more reproducible (91).

Summarizing diastolic function assessment. The Canadian Consensus on Diastolic Dysfunction (92) has defined 3 stages of diastolic dysfunction using standard PW Doppler (Table 1), which reflect increasing LV chamber stiffness and elevated left atrial pressure that lead to heart failure symptoms and correlate with patients' outcome. Because a classification based solely on mitral and pulmonary vein flow is sometimes equivocal, we have proposed additional criteria using color M-mode and DTI data (93). Further refinements include preload decrease maneuvers to substratify restrictive filling stage into reversible (where preload decrease results in normalization of filling) and irreversible stages. Finally, newer markers of diastolic function (based on strain rate imaging or intraventricular pressure gradient measurements) may bring even more refinement to the classification of diastolic function.

ESTIMATION OF INVASIVE INDEXES OF DIASTOLIC FUNCTION

Moving beyond the qualitative assessment of diastolic function described in the preceding text, we turn to more quantitative estimates of invasive diastolic function param-

Table 2. Proposed Equations for Estimating Filling Pressures and Corresponding Limits of Agreement

Authors	Equations	R Value	95% LOA
Mulvagh et al. (106)	46 − 0.22 IVRT − 0.10 AFF − 0.03 DT − 2A/E + 0.05 MAR	0.80	±7.4*
Garcia et al. (104)	$5.27 \times [E/V_p] + 4.6$	0.80	−5.1–5.3
Stein et al. (102)	Diastolic pressure − $4V_{MR\text{-}AVO^2}$	0.97	−1.2–7.4
Nagueh et al. (103)	$1.91 + 1.24 \times E/E_a$	0.87	−7.5–7.7
Rivas-Gotz et al. (98)	$0.9 \times$ systolic pressure $\times e^{-IVRT/tau(Ea-E)}$	0.84	−5.9–8.1

*Only standard error of the estimate of the linear regression is reported.

A = A-wave velocity; AFF = atrial filling fraction; DT = deceleration time; E = E-wave velocity; Ea = E-wave velocity by Doppler tissue at mitral annulus; IVRT = isovolumic relaxation time; LOA = limits of agreement; MAR = time from termination of mitral flow to the electrocardiographic R wave; tau(Ea−E) = tau estimated from the time difference between the E-wave onset recorded by standard and tissue Doppler; $V_{MR\text{-}AVO}$ = mitral regurgitation velocity at the time of mitral valve opening; V_p = color M-mode flow propagation velocity.

JACC Vol. 48, No. 10, 2006
November 21, 2006:2012–25

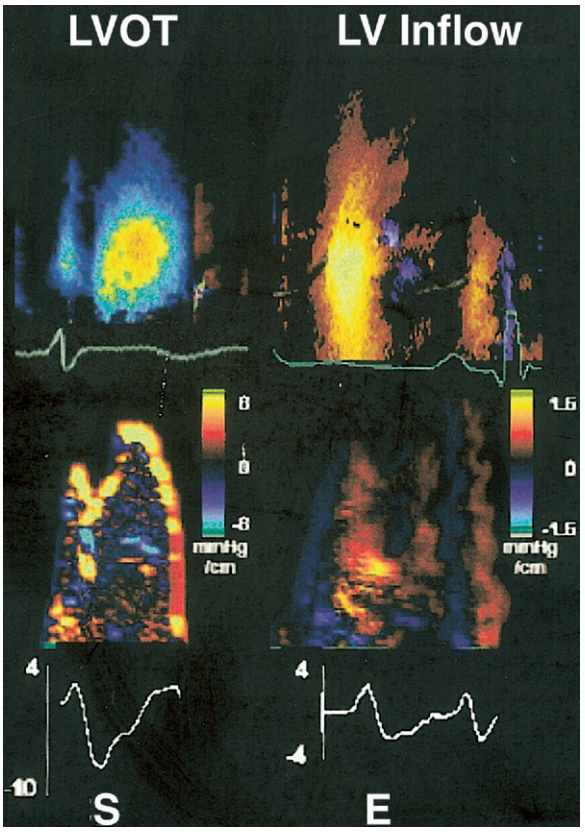

Figure 7. A standard time/velocity map obtained by color M-mode **(top)**; a time/pressure gradient map generated from color M-mode data by solving Euler equation **(middle)**; and tracings of intraventricular pressure differences obtained by integration of time/pressure gradient map **(bottom)**. E = peak early diastolic gradient obtained from left ventricular inflow; LV = left ventricular; LVOT = left ventricular outflow tract; S = peak systolic gradient obtained from the LVOT.

eters like relaxation, compliance, filling pressure, and diastolic suction (intraventricular pressure gradient).

Relaxation. The time constant of isovolumic pressure decay, or tau, represents a reference invasive measure for relaxation. Tau can be estimated from the isovolumetric relaxation time (IVRT) using the simplified equation:

$$\text{tau} = \text{IVRT} / \left[\ln(\text{systolic pressure}) - \ln(\text{filling pressure})\right]$$

with filling pressure measured invasively, estimated noninvasively (see the following text), or assuming a filling pressure of 10 mm Hg for patients not in heart failure (94). Also, several other surrogates of tau can be assessed by echocardiography. These include isovolumic relaxation time itself (95), the color M-mode flow propagation velocity (96), early myocardial relaxation velocity (97), and the time difference between the E-wave onset recorded by PW Doppler and by PW DTI at the mitral annulus (98).

LV compliance. In vitro and theoretical analysis predicts that the deceleration time of the E wave is shortened by low LV operating compliance (76). Animal (99) and clinical (100) work has validated this concept, which likely explains the poor prognosis of the restrictive filling pattern (80,81).

Filling pressures. Most of the numerous methods to estimate LV filling pressures are empirical, because there is no physical relationship that can be used to extract absolute pressures echocardiographic data. One exception is estimating left atrial pressure by subtracting the peak LV-left atrial pressure difference (obtained from continuous wave Doppler of mitral regurgitation) from systolic blood pressure, a method with high relative error because we must subtract 2 large numbers, each with their own intrinsic error, to yield a small number (101,102). Other approaches that have some theoretical underpinnings recognize that E velocity is proportional to (left atrial pressure)/tau, whereas annular E-wave (Ea) and color M-mode velocity of propagation (Vp) are assumed load-independent and inversely related to tau. Thus, both E/Ea (103) and E/Vp (104) have been shown to be linearly related to left atrial pressure. Other proposed estimation methods have used mitral E-wave deceleration time (105), a multiple regression model that incorporates several predictors (106) and differences in the timing of the E-wave onset recorded by standard, as opposed to tissue, PW Doppler (98). Of interest, this last method is based on manipulation of a simplified tau equation (98) (Table 2). One has to be reminded that although all of the methods showed promise in initial

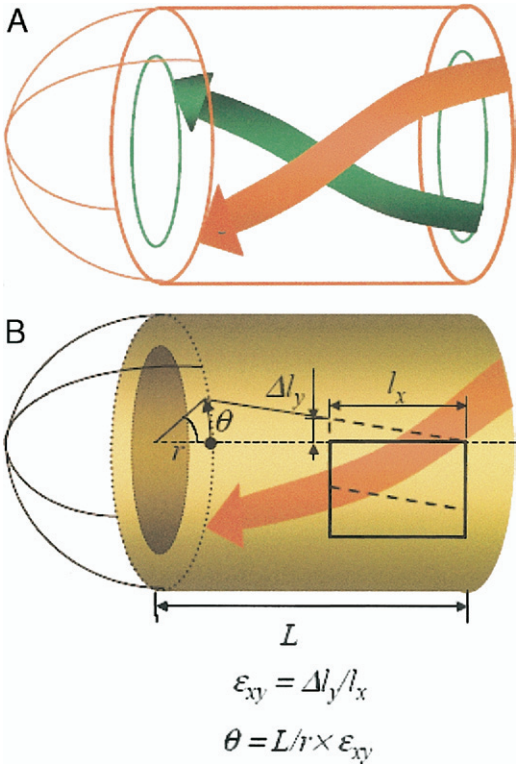

Figure 8. (A) Diagram depicting left-helix orientation of epicardial **(red)** and right helix orientation of endocardial **(green)** fibers within the myocardial shell. Epicardial fibers lay farther outward and are more numerous than endocardial fibers. The result of this imbalance is that, during contraction, shear strain occurs in a direction of the epicardial fiber orientation. **(B)** Relationship between shear strain ϵxy and torsion θ. Shear strain is generated by a contraction of epicardial fibers oriented in left-handed helix **(light red arrow)**. Torsion is proportional to shear strain and ventricular length, and inversely proportional to short-axis radius.

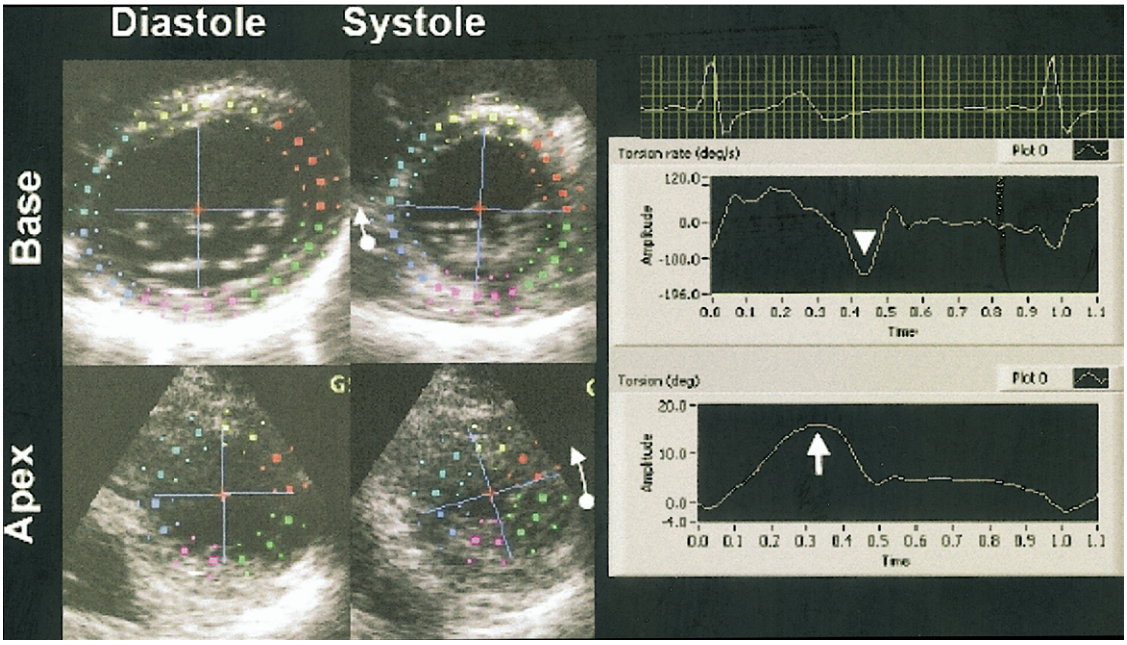

Figure 9. Quantitation of torsion and torsion velocity (rate) by speckle tracking imaging. Images to the **left** represent cross-sectional views of the base and the apex of the left ventricle superimposed with speckle tracking imaging-generated markers of left ventricular torsion. Images to the **right** represent torsion rate and torsion signal. **Arrowhead** and **arrow** mark peak negative torsion velocity and peak systolic torsion, respectively.

reports, frequently contradictory data emerge in duplication studies. Also, DTI and color M-mode indexes are not entirely preload-independent, particularly in normal hearts. Finally, in all of the studies, limits of agreement between echocardiography-derived estimates and invasive standards were 5 mm Hg or more, indicating that echocardiographic filling pressures are still just estimates.

Intraventricular pressure differences. Studies over the past 25 years have shown the existence of small (2 to 4 mm Hg) pressure differences between the base and the apex of the LV during early diastole (107), which facilitate efficient filling by keeping filling pressure low. Importantly, these are eliminated by ischemia (108) and other pathologies, but their actual invasive measurement is so complex as to preclude clinical use. A recent development in this area is the ability to calculate atrioventricular and intraventricular pressure gradients completely non-invasively by applying the Euler equation to the color M-mode velocity profile (Fig. 7). The Euler equation requires a spatiotemporal velocity map v(s,t) of flow along a streamline and yields the rate of change of pressure along that streamline of flow. The first of the 2 elements of the equation represents an inertial term related to acceleration of blood, whereas the second term reflects the conversion of potential to kinetic energy by convection. Note that all we need to solve this equation is a representation of velocity as a function of space and time, which is precisely what the color M-mode is. The Euler equation is closely related to the Bernoulli equation, which yields the total pressure drop across a discrete stenosis. Integrating the Euler equation from the base to the apex yields the intraventricular pressure difference. This non-invasive approach has been validated in animals (109) and in patients with hypertrophic cardiomyopathy, demonstrating a significant improvement in diastolic suction with successful alcohol septal ablation (110). Intraventricular pressure difference has been shown to be low in patients with dilated cardiomyopathy (111), whereas the augmentation of suction has also proven highly predictive of exercise capacity in normal subjects and heart failure patients (112). As noted in the preceding text, intraventricular pressure difference measurements along the LVOT have been shown to estimate systolic function accurately.

Shear strain and torsion. One of the intriguing aspects of the complex fiber architecture of the LV is how it produces shearing and torsion of the ventricle, similar to wringing a towel dry. Shear strain appears when a force acts parallel to the reference plane, leading to a change of shape. Figures 8A and 8B illustrate the link between myocardial structure, shear strain, and torsion. A simple way to think of torsion is the difference in rotation between the base and apex of the heart. Viewed from the apex, left-handed epicardial fiber helix tries to pull the apex counterclockwise and the base clockwise. The right-handed helix in the endocardium does the opposite, but because the epicardium is farther from the centerline, its torque is greater and thus it dominates the twisting (113), leading to about a 12° difference between base and apex.

Though a fundamental measure of LV mechanics, torsion measurement has previously required sophisticated magnetic resonance tagging (114). We have recently developed 2 echocardiographic methods for quantifying torsion, one based on DTI (115), the other, recently confirmed, based on STI (116,117). The STI method is easier, but with lower time resolution (Fig. 9). A cross-sectional study of subjects

from newborn to 50 years showed maturational changes in torsion, with the heart rotating clockwise essentially as a solid body in infancy, developing the adult pattern of torsion by adolescence (118). Torsion appears to be a critical link between systole and diastole, with elastic energy stored during systole, then abruptly released with sudden untwisting during isovolumic relaxation, generating intraventricular pressure gradients and allowing filling to proceed at low filling pressure. This is particularly important during the disproportionately shortened diastole of exercise. We have shown that the untwisting rate is highly correlated with intraventricular pressure difference at rest and exercise, a relationship that holds both in health and in presence of hypertrophic cardiomyopathy (119).

WHAT TO DO WHEN?

Which of these myriad measurements should be made in routine echocardiographic practice? No laboratory can afford to do all of these either in acquisition or interpretation, but general guidelines may be offered, balancing those measurements that are easiest to make and give the greatest value. We feel that end-diastolic and -systolic volumes should be measured, ideally by 3D but acceptably by 2D echocardiography and Simpson's rule, from which EF and SV can be calculated. Stroke volume should also be measured directly by PW Doppler in the LVOT. Color and continuous wave Doppler should be obtained through every valve to seek occult stenosis or regurgitation. If stenotic, valve area should be calculated by continuity or planimetry; for mitral or tricuspid regurgitation, a proximal convergence zone should be sought and analyzed, whereas for aortic, flow reversal in the aortic arch is a useful adjunct to regurgitant jet appearance. Diastolic function should be assessed with PW Doppler at the mitral leaflet tips and pulmonary vein, PW DTI at the lateral annulus, and color M-mode flow propagation, the latter 2 of which may often be judged qualitatively (low/high, slow/fast) for a quick separation of normal from pseudonormal pattern. Left atrial area and/or volume are an indispensable part of final diastolic function report. Regional wall motion should be qualitatively assessed globally and segment-by-segment, and, if available, (semi)automated analysis methods may make this more reproducible. Advanced methods like torsion and intraventricular pressure gradients are promising, but beyond the scope of routine clinical practice. It is hoped that ultrasound manufacturers will develop accessible user interfaces to bring these techniques into common practice as they have done with previously arcane methods like the continuity equation and pressure half-times.

CONCLUSIONS

In summary, Doppler echocardiography has proven to be the most versatile cardiovascular imaging modality, providing a comprehensive assessment of valvular and ventricular hemodynamics and global and regional systolic and diastolic function. With improvements in transducer technology and the relentless doubling of computer speed every 18 months, we can only expect ever more precise echocardiographic assessment of cardiac mechanics.

Reprint requests and correspondence: Dr. James D. Thomas, Department of Cardiology, Desk F-15, The Cleveland Clinic Foundation, 9500 Euclid Avenue, Cleveland, Ohio 44195. E-mail: thomasj@ccf.org.

REFERENCES

1. Marwick TH. Stress echocardiography. Heart 2003;89:113–8.
2. Lewis JF, Kuo LC, Nelson JG, Limacher MC, Quinones MA. Pulsed Doppler echocardiographic determination of stroke volume and cardiac output: clinical validation of two new methods using the apical window. Circulation 1984;70:425–31.
3. Dittmann H, Voelker W, Karsch KR, Seipel L. Influence of sampling site and flow area on cardiac output measurements by Doppler echocardiography. J Am Coll Cardiol 1987;10:818–23.
4. Kim WY, Poulsen JK, Terp K, Staalsen NH. A new Doppler method for quantification of volumetric flow: in vivo validation using color Doppler. J Am Coll Cardiol 1996;27:182–92.
5. Sun JP, Pu M, Fouad FM, Christian R, Stewart WJ, Thomas JD. Automated cardiac output measurement by spatiotemporal integration of color Doppler data. In vitro and clinical validation. Circulation 1997;95:932–9.
6. Meijboom EJ, Horowitz S, Valdes-Cruz LM, Sahn DJ, Larson DF, Oliveira Lima C. A Doppler echocardiographic method for calculating volume flow across the tricuspid valve: correlative laboratory and clinical studies. Circulation 1985;71:551–6.
7. Pu M, Griffin BP, Vandervoort PM, Leung DY, Cosgrove DM 3rd, Thomas JD. Intraoperative validation of mitral inflow determination by transesophageal echocardiography: comparison of single-plane, biplane and thermodilution techniques. J Am Coll Cardiol 1995;26:1047–53.
8. Kitabatake A, Inoue M, Asao M, et al. Noninvasive evaluation of the ratio of pulmonary to systemic flow in atrial septal defect by duplex Doppler echocardiography. Circulation 1984;69:73–9.
9. Kurokawa S, Takahashi M, Katoh Y, Muramatsu J, Kikawada R. Noninvasive evaluation of the ratio of pulmonary to systemic flow in ventricular septal defect by means of Doppler two-dimensional echocardiography. Am Heart J 1988;116:1033–44.
10. Enriquez-Sarano M, Bailey KR, Seward JB, Tajik AJ, Krohn MJ, Mays JM. Quantitative Doppler assessment of valvular regurgitation. Circulation 1993;87:841–8.
11. Bargiggia GS, Tronconi L, Sahn DJ, et al. A new method for quantitation of mitral regurgitation based on color flow Doppler imaging of flow convergence proximal to regurgitant orifice. Circulation 1991;84:1481–9.
12. Vandervoort PM, Rivera JM, Mele D, et al. Application of color Doppler flow mapping to calculate effective regurgitant orifice area. An in vitro study and initial clinical observations. Circulation 1993;88:1150–6.
13. Pu M, Prior DL, Fan X, et al. Calculation of mitral regurgitant orifice area with use of a simplified proximal convergence method: initial clinical application. J Am Soc Echocardiogr 2001;14:180–5.
14. Zhang J, Jones M, Shandas R, et al. Accuracy of flow convergence estimates of mitral regurgitant flow rates obtained by use of multiple color flow Doppler M-mode aliasing boundaries: an experimental animal study. Am Heart J 1993;125:449–58.
15. Pu M, Vandervoort PM, Griffin BP, et al. Quantification of mitral regurgitation by the proximal convergence method using transesophageal echocardiography. Clinical validation of a geometric correction for proximal flow constraint. Circulation 1995;92:2169–77.
16. Currie PJ, Seward JB, Reeder GS, et al. Continuous wave Doppler echocardiographic assessment of severity of calcific aortic stenosis: a simultaneous Doppler-catheter correlative study in 100 adult patients. Circulation 1985;71:1162–9.
17. Simon AC, Flaud P, Levenson J. Non-invasive evaluation of segmental pressure drop and resistance in large arteries in humans

based on a Poiseuille model of intra-arterial velocity distribution. Cardiovasc Res 1990;24:623–6.
18. Firstenberg MS, Vandervoort PM, Greenberg NL, et al. Noninvasive estimation of transmitral pressure drop across the normal mitral valve in humans: importance of convective and inertial forces during left ventricular filling. J Am Coll Cardiol 2000;36:1942–9.
19. Nakatani S, Firstenberg MS, Greenberg NL, et al. Mitral inertance in humans: critical factor in Doppler estimation of transvalvular pressure gradients. Am J Physiol Heart Circ Physiol 2001;280: H1340–5.
20. Vandervoort PM, Greenberg NL, Powell KA, Cosgrove DM, Thomas JD. Pressure recovery in bileaflet heart valve prostheses. Localized high velocities and gradients in central and side orifices with implications for Doppler-catheter gradient relation in aortic and mitral position. Circulation 1995;92:3464–72.
21. Popovic AD, Thomas JD, Neskovic AN, Cosgrove DM 3rd, Stewart WJ, Lauer MS. Time-related trends in the preoperative evaluation of patients with valvular stenosis. Am J Cardiol 1997;80:1464–8.
22. Thomas JD, Liu CM, Flachskampf FA, O'Shea JP, Davidoff R, Weyman AE. Quantification of jet flow by momentum analysis. An in vitro color Doppler flow study. Circulation 1990;81:247–59.
23. Cape EG, Skoufis EG, Weyman AE, Yoganathan AP, Levine RA. A new method for noninvasive quantification of valvular regurgitation based on conservation of momentum. In vitro validation. Circulation 1989;79:1343–53.
24. Mulvagh SL, DeMaria AN, Feinstein SB, et al. Contrast echocardiography: current and future applications. J Am Soc Echocardiogr 2000;13:331–42.
25. Bellenger NG, Burgess MI, Ray SG, et al. Comparison of left ventricular ejection fraction and volumes in heart failure by echocardiography, radionuclide ventriculography and cardiovascular magnetic resonance; are they interchangeable? Eur Heart J 2000;21: 1387–96.
26. Pombo JF, Troy BL, Russell RO Jr. Left ventricular volumes and ejection fraction by echocardiography. Circulation 1971;43:480–90.
27. Teichholz LE, Kreulen T, Herman MV, Gorlin R. Problems in echocardiographic volume determinations: echocardiographic-angiographic correlations in the presence of absence of asynergy. Am J Cardiol 1976;37:7–11.
28. Yvorchuk KJ, Davies RA, Chan KL. Measurement of left ventricular ejection fraction by acoustic quantification and comparison with radionuclide angiography. Am J Cardiol 1994;74:1052–6.
29. Mor-Avi V, Vignon P, Koch R, et al. Segmental analysis of color kinesis images: new method for quantification of the magnitude and timing of endocardial motion during left ventricular systole and diastole. Circulation 1997;95:2082–97.
30. Chen CH, Nevo E, Fetics B, et al. Comparison of continuous left ventricular volumes by transthoracic two-dimensional digital echo quantification with simultaneous conductance catheter measurements in patients with cardiac diseases. Am J Cardiol 1997;80:756–61.
31. Qin JX, Jones M, Shiota T, et al. Validation of real-time three-dimensional echocardiography for quantifying left ventricular volumes in the presence of a left ventricular aneurysm: in vitro and in vivo studies. J Am Coll Cardiol 2000;36:900–7.
32. Bauer F, Jones M, Qin JX, et al. Quantitative analysis of left atrial function during left ventricular ischemia with and without left atrial ischemia: a real-time 3-dimensional echocardiographic study. J Am Soc Echocardiogr 2005;18:795–801.
33. Mor-Avi V, Sugeng L, Weinert L, et al. Fast measurement of left ventricular mass with real-time three-dimensional echocardiography: comparison with magnetic resonance imaging. Circulation 2004;110: 1814–8.
34. Jenkins C, Bricknell K, Hanekom L, Marwick TH. Reproducibility and accuracy of echocardiographic measurements of left ventricular parameters using real-time three-dimensional echocardiography. J Am Coll Cardiol 2004;44:878–86.
35. Tanabe K, Belohlavek M, Jakrapanichakul D, Bae RY, Greenleaf JF, Seward JB. Three-dimensional echocardiography: precision and accuracy of left ventricular volume measurement using rotational geometry with variable numbers of slice resolution. Echocardiography 1998;15:575–80.
36. Corsi C, Lang RM, Veronesi F, et al. Volumetric quantification of global and regional left ventricular function from real-time three-dimensional echocardiographic images. Circulation 2005; 112:1161–70.
37. Suga H, Sagawa K. Instantaneous pressure-volume relationships and their ratio in the excised, supported canine left ventricle. Circ Res 1974;35:117–26.
38. Kass DA, Beyar R. Evaluation of contractile state by maximal ventricular power divided by the square of end-diastolic volume. Circulation 1991;84:1698–708.
39. Nakayama M, Chen CH, Nevo E, Fetics B, Wong E, Kass DA. Optimal preload adjustment of maximal ventricular power index varies with cardiac chamber size. Am Heart J 1998;136:281–8.
40. Segers P, Tchana-Sato V, Leather HA, et al. Determinants of left ventricular preload-adjusted maximal power. Am J Physiol Heart Circ Physiol 2003;284:H2295–301.
41. Chen CH, Fetics B, Nevo E, et al. Noninvasive single-beat determination of left ventricular end-systolic elastance in humans. J Am Coll Cardiol 2001;38:2028–34.
42. Kawaguchi M, Hay I, Fetics B, Kass DA. Combined ventricular systolic and arterial stiffening in patients with heart failure and preserved ejection fraction: implications for systolic and diastolic reserve limitations. Circulation 2003;107:714–20.
43. Bauer F, Jones J, Shiota T, et al. Left ventricular outflow tract mean systolic acceleration as a surrogate for the slope of the left ventricular end-systolic pressure-volume relationship. J Am Coll Cardiol 2002; 40:1320–7.
44. Greenberg NL, Firstenberg MS, Castro PL, et al. Doppler-derived myocardial systolic strain rate is a strong index of left ventricular contractility. Circulation 2002;105:99–105.
45. Yotti R, Bermejo J, Desco MM, et al. Doppler-derived ejection intraventricular pressure gradients provide a reliable assessment of left ventricular systolic chamber function. Circulation 2005;112:1771–9.
46. Parthenakis FI, Kanakaraki MK, Kanoupakis EM, et al. Value of Doppler index combining systolic and diastolic myocardial performance in predicting cardiopulmonary exercise capacity in patients with congestive heart failure: effects of dobutamine. Chest 2002;121: 1935–41.
47. Cheung MM, Smallhorn JF, Redington AN, Vogel M. The effects of changes in loading conditions and modulation of inotropic state on the myocardial performance index: comparison with conductance catheter measurements. Eur Heart J 2004;25:2238–42.
48. Vogel M, Schmidt MR, Kristiansen SB, et al. Validation of myocardial acceleration during isovolumic contraction as a novel noninvasive index of right ventricular contractility: comparison with ventricular pressure-volume relations in an animal model. Circulation 2002;105: 1693–9.
49. Lyseggen E, Rabben SI, Skulstad H, Urheim S, Risoe C, Smiseth OA. Myocardial acceleration during isovolumic contraction: relationship to contractility. Circulation 2005;111:1362–9.
50. Lang RM, Bierig M, Devereux RB, et al. Recommendations for chamber quantification: a report from the American Society of Echocardiography's Guidelines and Standards Committee and the Chamber Quantification Writing Group, developed in conjunction with the European Association of Echocardiography, a branch of the European Society of Cardiology. J Am Soc Echocardiogr 2005;18: 1440–63.
51. Heger JJ, Weyman AE, Wann LS, Dillon JC, Feigenbaum H. Cross-sectional echocardiography in acute myocardial infarction: detection and localization of regional left ventricular asynergy. Circulation 1979;60:531–8.
52. Costa KD, Takayama Y, McCulloch AD, Covell JW. Laminar fiber architecture and three-dimensional systolic mechanics in canine ventricular myocardium. Am J Physiol 1999;276:H595–607.
53. Arts T, Costa KD, Covell JW, McCulloch AD. Relating myocardial laminar architecture to shear strain and muscle fiber orientation. Am J Physiol Heart Circ Physiol 2001;280:H2222–9.
54. Chen J, Liu W, Zhang H, et al. Regional ventricular wall thickening reflects changes in cardiac fiber and sheet structure during contraction: quantification with diffusion tensor MRI. Am J Physiol Heart Circ Physiol 2005;289:H1898–907.
55. Spotnitz HM, Spotnitz WD, Cottrell TS, Spiro D, Sonnenblick EH. Cellular basis for volume related wall thickness changes in the rat left ventricle. J Mol Cell Cardiol 1974;6:317–31.
56. Harrington KB, Rodriguez F, Cheng A, et al. Direct measurement of transmural laminar architecture in the anterolateral wall of the ovine

left ventricle: new implications for wall thickening mechanics. Am J Physiol Heart Circ Physiol 2005;288:H1324–30.
57. MacGowan GA, Shapiro EP, Azhari H, et al. Noninvasive measurement of shortening in the fiber and cross-fiber directions in the normal human left ventricle and in idiopathic dilated cardiomyopathy. Circulation 1997;96:535–41.
58. Popovic ZB, Grimm RA, Perlic G, et al. Noninvasive assessment of cardiac resynchronization therapy for congestive heart failure using myocardial strain and left ventricular peak power as parameters of myocardial synchrony and function. J Cardiovasc Electrophysiol 2002;13:1203–8.
59. Yu CM, Chau E, Sanderson JE, et al. Tissue Doppler echocardiographic evidence of reverse remodeling and improved synchronicity by simultaneously delaying regional contraction after biventricular pacing therapy in heart failure. Circulation 2002;105:438–45.
60. Bax JJ, Abraham T, Barold SS, et al. Cardiac resynchronization therapy: part 1—issues before device implantation. J Am Coll Cardiol 2005;46:2153–67.
61. Marwick TH, Case C, Leano R, et al. Use of tissue Doppler imaging to facilitate the prediction of events in patients with abnormal left ventricular function by dobutamine echocardiography. Am J Cardiol 2004;93:142–6.
62. Iwasaki Y, Satomi G, Yasukochi S. Analysis of ventricular septal motion by Doppler tissue imaging in atrial septal defect and normal heart. Am J Cardiol 1999;83:206–10.
63. D'Hooge J, Heimdal A, Jamal F, et al. Regional strain and strain rate measurements by cardiac ultrasound: principles, implementation and limitations. Eur J Echocardiogr 2000;1:154–70.
64. Glantz SA, Parmley WW. Factors which affect the diastolic pressure-volume curve. Circ Res 1978;42:171–80.
65. Edvardsen T, Gerber BL, Garot J, Bluemke DA, Lima JA, Smiseth OA. Quantitative assessment of intrinsic regional myocardial deformation by Doppler strain rate echocardiography in humans: validation against three-dimensional tagged magnetic resonance imaging. Circulation 2002;106:50–6.
66. Voigt JU, Exner B, Schmiedehausen K, et al. Strain-rate imaging during dobutamine stress echocardiography provides objective evidence of inducible ischemia. Circulation 2003;107:2120–6.
67. Hoffmann R, Altiok E, Nowak B, et al. Strain rate measurement by Doppler echocardiography allows improved assessment of myocardial viability in patients with depressed left ventricular function. J Am Coll Cardiol 2002;39:443–9.
68. Sun JP, Popovic ZB, Greenberg NL, et al. Noninvasive quantification of regional myocardial function using Doppler-derived velocity, displacement, strain rate, and strain in healthy volunteers: effects of aging. J Am Soc Echocardiogr 2004;17:132–8.
69. Urheim S, Edvardsen T, Torp H, Angelsen B, Smiseth OA. Myocardial strain by Doppler echocardiography. Validation of a new method to quantify regional myocardial function. Circulation 2000; 102:1158–64.
70. Amundsen BH, Helle-Valle T, Edvardsen T, et al. Noninvasive myocardial strain measurement by speckle tracking echocardiography validation against sonomicrometry and tagged magnetic resonance imaging. J Am Coll Cardiol 2006;47:789–93.
71. Suffoletto MS, Dohi K, Cannesson M, Saba S, Gorcsan J 3rd. Novel speckle-tracking radial strain from routine black-and-white echocardiographic images to quantify dyssynchrony and predict response to cardiac resynchronization therapy. Circulation 2006;113:960–8.
72. Zhang Y, Chan AK, Yu CM, et al. Strain rate imaging differentiates transmural from non-transmural myocardial infarction: a validation study using delayed-enhancement magnetic resonance imaging. J Am Coll Cardiol 2005;46:864–71.
73. Hanekom L, Jenkins C, Jeffries L, et al. Incremental value of strain rate analysis as an adjunct to wall-motion scoring for assessment of myocardial viability by dobutamine echocardiography: a follow-up study after revascularization. Circulation 2005;112:3892–900.
74. Skulstad H, Urheim S, Edvardsen T, et al. Grading of myocardial dysfunction by tissue Doppler echocardiography: a comparison between velocity, displacement, and strain imaging in acute ischemia. J Am Coll Cardiol 2006;47:1672–82.
75. Vitarelli A, Montesano T, Gaudio C, et al. Strain rate dobutamine echocardiography for prediction of recovery after revascularization in patients with ischemic left ventricular dysfunction. J Card Fail 2006;12:268–75.
76. Thomas JD, Weyman AE. Echocardiographic Doppler evaluation of left ventricular diastolic function. Physics and physiology. Circulation 1991;84:977–90.
77. Thomas JD, Weyman AE. Doppler mitral pressure half-time: a clinical tool in search of theoretical justification. J Am Coll Cardiol 1987;10:923–9.
78. Choong CY, Abascal VM, Thomas JD, Guerrero JL, McGlew S, Weyman AE. Combined influence of ventricular loading and relaxation on the transmitral flow velocity profile in dogs measured by Doppler echocardiography. Circulation 1988;78:672–83.
79. Thomas JD, Choong CY, Flachskampf FA, Weyman AE. Analysis of the early transmitral Doppler velocity curve: effect of primary physiologic changes and compensatory preload adjustment. J Am Coll Cardiol 1990;16:644–55.
80. Klein AL, Hatle LK, Taliercio CP, et al. Prognostic significance of Doppler measures of diastolic function in cardiac amyloidosis. A Doppler echocardiography study. Circulation 1991;83:808–16.
81. Xie GY, Berk MR, Smith MD, Gurley JC, DeMaria AN. Prognostic value of Doppler transmitral flow patterns in patients with congestive heart failure. J Am Coll Cardiol 1994;24:132–9.
82. Tabata T, Thomas JD, Klein AL. Pulmonary venous flow by Doppler echocardiography: revisited 12 years later. J Am Coll Cardiol 2003; 41:1243–50.
83. Thomas JD, Zhou J, Greenberg N, Bibawy G, McCarthy PM, Vandervoort PM. Physical and physiological determinants of pulmonary venous flow: numerical analysis. Am J Physiol 1997; 272:H2453–65.
84. Rossvoll O, Hatle LK. Pulmonary venous flow velocities recorded by transthoracic Doppler ultrasound: relation to left ventricular diastolic pressures. J Am Coll Cardiol 1993;21:1687–96.
85. Sohn DW, Chai IH, Lee DJ, et al. Assessment of mitral annulus velocity by Doppler tissue imaging in the evaluation of left ventricular diastolic function. J Am Coll Cardiol 1997;30:474–80.
86. Garcia MJ, Rodriguez L, Ares M, Griffin BP, Thomas JD, Klein AL. Differentiation of constrictive pericarditis from restrictive cardiomyopathy: assessment of left ventricular diastolic velocities in longitudinal axis by Doppler tissue imaging. J Am Coll Cardiol 1996;27: 108–14.
87. Brun P, Tribouilloy C, Duval AM, Iserin L, Meguira A. Left ventricular flow propagation during early filling is related to wall relaxation: a color M-mode Doppler analysis. J Am Coll Cardiol 1992;20:420–32.
88. Stugaard M, Risoe C, Ihlen H, Smiseth OA. Intracavitary filling pattern in the failing left ventricle assessed by color M-mode echocardiography. J Am Coll Cardiol 1994;24:663–70.
89. Stugaard M, Smiseth OA, Risoe C, Ihlen H. Intraventricular early diastolic filling during acute myocardial ischemia: assessment by multigated color M-mode Doppler echocardiography. Circulation 1993;88:2705–13.
90. Takatsuji H, Mikami T, Urasawa K, et al. A new approach for evaluation of left ventricular diastolic function: spatial and temporal analysis of left ventricular filling flow propagation by color M-mode Doppler echocardiography. J Am Coll Cardiol 1996;27:365–71.
91. Greenberg NL, Firstenberg MS, Cardon LA, et al. Automated assessment of noninvasive filling pressure using color Doppler M-mode echocardiography. Comput Cardiol 2001;28:601–4.
92. Rakowski H, Appleton C, Chan KL, et al. Canadian consensus recommendations for the measurement and reporting of diastolic dysfunction by echocardiography: from the Investigators of Consensus on Diastolic Dysfunction by Echocardiography. J Am Soc Echocardiogr 1996;9:736–60.
93. Garcia MJ, Thomas JD, Klein AL. New Doppler echocardiographic applications for the study of diastolic function. J Am Coll Cardiol 1998;32:865–75.
94. Scalia GM, Greenberg NL, McCarthy PM, Thomas JD, Vandervoort PM. Noninvasive assessment of the ventricular relaxation time constant (tau) in humans by Doppler echocardiography. Circulation 1997;95:151–5.
95. Thomas JD, Flachskampf FA, Chen C, et al. Isovolumic relaxation time varies predictably with its time constant and aortic and left atrial pressures: implications for the noninvasive evaluation of ventricular relaxation. Am Heart J 1992;124:1305–13.
96. Garcia MJ, Smedira NG, Greenberg NL, et al. Color M-mode Doppler flow propagation velocity is a preload insensitive index of left

ventricular relaxation: animal and human validation. J Am Coll Cardiol 2000;35:201–8.
97. Oki T, Tabata T, Yamada H, et al. Clinical application of pulsed Doppler tissue imaging for assessing abnormal left ventricular relaxation. Am J Cardiol 1997;79:921–8.
98. Rivas-Gotz C, Khoury DS, Manolios M, Rao L, Kopelen HA, Nagueh SF. Time interval between onset of mitral inflow and onset of early diastolic velocity by tissue Doppler: a novel index of left ventricular relaxation: experimental studies and clinical application. J Am Coll Cardiol 2003;42:1463–70.
99. Little WC, Ohno M, Kitzman DW, Thomas JD, Cheng CP. Determination of left ventricular chamber stiffness from the time for deceleration of early left ventricular filling. Circulation 1995;92: 1933–9.
100. Garcia MJ, Firstenberg MS, Greenberg NL, et al. Estimation of left ventricular operating stiffness from Doppler early filling deceleration time in humans. Am J Physiol Heart Circ Physiol 2001;280: H554–61.
101. Pozzoli M. Non-invasive evaluation of the hemodynamic profile in patients with heart failure: estimation of left atrial pressure (in Italian). Ital Heart J Suppl 2000;1:1326–33.
102. Stein JH, Neumann A, Preston LM, et al. Echocardiography for hemodynamic assessment of patients with advanced heart failure and potential heart transplant recipients. J Am Coll Cardiol 1997;30: 1765–72.
103. Nagueh SF, Mikati I, Kopelen HA, Middleton KJ, Quinones MA, Zoghbi WA. Doppler estimation of left ventricular filling pressure in sinus tachycardia. A new application of tissue Doppler imaging. Circulation 1998;98:1644–50.
104. Garcia MJ, Ares MA, Asher C, Rodriguez L, Vandervoort P, Thomas JD. An index of early left ventricular filling that combined with pulsed Doppler peak E velocity may estimate capillary wedge pressure. J Am Coll Cardiol 1997;29:448–54.
105. Giannuzzi P, Imparato A, Temporelli PL, et al. Doppler-derived mitral deceleration time of early filling as a strong predictor of pulmonary capillary wedge pressure in postinfarction patients with left ventricular systolic dysfunction. J Am Coll Cardiol 1994;23: 1630–7.
106. Mulvagh S, Quinones MA, Kleiman NS, Cheirif J, Zoghbi WA. Estimation of left ventricular end-diastolic pressure from Doppler transmitral flow velocity in cardiac patients independent of systolic performance. J Am Coll Cardiol 1992;20:112–9.
107. Ling D, Rankin JS, Edwards CH 2nd, McHale PA, Anderson RW. Regional diastolic mechanics of the left ventricle in the conscious dog. Am J Physiol 1979;236:H323–30.
108. Courtois M, Kovacs SJ, Ludbrook PA. Physiological early diastolic intraventricular pressure gradient is lost during acute myocardial ischemia. Circulation 1990;81:1688–96.
109. Greenberg NL, Vandervoort PM, Firstenberg MS, Garcia MJ, Thomas JD. Estimation of diastolic intraventricular pressure gradients by Doppler M-mode echocardiography. Am J Physiol Heart Circ Physiol 2001;280:H2507–15.
110. Rovner A, Smith R, Greenberg NL, et al. Improvement in diastolic intraventricular pressure gradients in patients with HOCM after ethanol septal reduction. Am J Physiol Heart Circ Physiol 2003;285: H2492–9.
111. Yotti R, Bermejo J, Antoranz JC, et al. A noninvasive method for assessing impaired diastolic suction in patients with dilated cardiomyopathy. Circulation 2005;112:2921–9.
112. Rovner A, Greenberg NL, Thomas JD, Garcia MJ. Relationship of diastolic intraventricular pressure gradients and aerobic capacity in patients with diastolic heart failure. Am J Physiol Heart Circ Physiol 2005;289:H2081–8.
113. Ingels NB Jr., Hansen DE, Daughters GT 2nd, Stinson EB, Alderman EL, Miller DC. Relation between longitudinal, circumferential, and oblique shortening and torsional deformation in the left ventricle of the transplanted human heart. Circ Res 1989;64:915–27.
114. Dong SJ, Hees PS, Siu CO, Weiss JL, Shapiro EP. MRI assessment of LV relaxation by untwisting rate: a new isovolumic phase measure of tau. Am J Physiol Heart Circ Physiol 2001;281:H2002–9.
115. Notomi Y, Setser RM, Shiota T, et al. Assessment of left ventricular torsional deformation by Doppler tissue imaging: validation study with tagged magnetic resonance imaging. Circulation 2005;111: 1141–7.
116. Notomi Y, Lysyansky P, Setser RM, et al. Measurement of ventricular torsion by two-dimensional ultrasound speckle tracking imaging. J Am Coll Cardiol 2005;45:2034–41.
117. Helle-Valle T, Crosby J, Edvardsen T, et al. New noninvasive method for assessment of left ventricular rotation: speckle tracking echocardiography. Circulation 2005;112:3149–56.
118. Notomi Y, Srinath G, Shiota T, et al. Maturational and adaptive modulation of left ventricular torsional biomechanics: Doppler tissue imaging observation from infancy to adulthood. Circulation 2006; 113:2534–41.
119. Notomi Y, Martin-Miklovic MG, Oryszak SJ, et al. Enhanced ventricular untwisting during exercise: a mechanistic manifestation of elastic recoil described by Doppler tissue imaging. Circulation 2006; 113:2524–33.